Interface Development and Encapsulation in Simultaneous Coinjection Molding. I. Two-Dimensional Modeling and Formulation

C. T. Li, A. I. Isayev

Institute of Polymer Engineering, University of Akron, Akron, Ohio 44325-0301

Received 14 March 2002; revised 22 July 2002; accepted 23 July 2002

ABSTRACT: In the coinjection-molding process two polymers are injected into a mold sequentially or simultaneously. During the process one polymer melt forms the skin and the other forms the core, resulting in an encapsulated sandwich structure. In an attempt to develop a process model and simulation of simultaneous coinjection molding, along with the interface treatment a theoretical approach, physical model, and numerical algorithm were formulated based on the Hele–Shaw approximation. A detailed picture of the dynamics and kinematics of the interface evolution, providing a description of the multilayer flow and interface development during the multicomponent injection-molding process, information typically lacking in the available literature, is systematically presented. Based on the developed numerical simulation code, the moldability of various material combinations can be evaluated, which is required for process optimization. © 2003 Wiley Periodicals, Inc. J Appl Polym Sci 88: 2300–2309, 2003

Key words: coinjection molding; interface kinematics and dynamics; finite element; finite difference; simulation; rheology

INTRODUCTION

The coinjection-molding process, also called sandwich injection molding, is one of the innovative multicomponent injection-molding processes. The sandwich injection-molding process was first patented in 1969.[1] Originally it was developed as an alternative to the structural foam process, using a cellular core combined with a solid skin in order to obtain a very good surface quality. The process has been commercially used since 1975.

In the coinjection-molding process, two or more polymers are injected into the cavity simultaneously or sequentially, such that the core material is embedded within the skin material, resulting in an encapsulated sandwich–structure product. The advantages offered by such a structure are akin to those derived from coextruded sheets and films and bicomponent fibers. Coinjection molding eliminates many of the manufacturing steps required by conventional lamination and coating processes, combining the desired properties of two or more polymers by melt fabrication.

In the coinjection-molding process different properties of the skin and core polymers and their distribution in the cavity greatly affect the properties and applications of moldings. Specific polymers for the skin layer can be selected in order to improve appearance and texture, strength, chemical resistance, EMI shielding, and other properties, while the core layer is composed of recycled or inexpensive material. The quality of the parts can be improved at lower cost.

There are two main techniques for doing coinjection molding: single channel and two channel. The single-channel technique[1–3] features a control valve that lets the melts enter the cavity sequentially. The two-channel technique[4–6] involves the simultaneous phase of injection of both skin and core materials after first injecting skin material. The one-channel technique's shortcomings are pressure drop and stagnation at the switchover point, resulting in a distinct "hesitation line" in the shape of a dull ring.[7,8] In addition, uneven distribution of the core material is usually seen in the sequential coinjection parts. Hence, the process is mainly used for manufacturing thick parts with a foamed core.

These disadvantages have been overcome by the two-channel technique. The simultaneous phase of injection of both skin and core allows control of the distribution of the core materials, as well as the avoidance of flow marks and differences in gloss by maintaining a constant flow-front velocity.[7] However, simultaneous coinjection was more difficult to control and required time-consuming trials. The most difficult task for an operator is finding the proper injection stroke for the simultaneous phase and the injection speed of the two materials.[8] At present, simulation of

Correspondence to: A. I. Isayev (aisayev@uakron.edu).
Contract grant sponsor: Lord Corporation.

Journal of Applied Polymer Science, Vol. 88, 2300–2309 (2003)

mold filling for the simultaneous coinjection-molding process is not available; profile settings, which optimize the process, are obtained only by trial and error. The optimization task becomes tedious when dealing with a new product for which little experience has been acquired.

Modeling of the coinjection-molding process is a relatively recent undertaking. A few numerical simulations of the coinjection-molding process have been attempted.[9–24] All these efforts were based on the use of the Hele–Shaw approximation to predict the interface evolution between the skin and core materials during filling for sequential coinjection, with the exception of Lee et. al.,[24] who considered a simultaneous coinjection process.

Lanvers et al.[9,10] presented a refinement of the model, describing the penetration behavior of the core component into the skin component with a phenomenological formulation whose coefficients were determined approximately from the MFI value of each individual component. Michaeli and Galuschka[11] applied the same phenomenological formula to their coinjection-molding simulation program. The basis of their approach was that the contour of the core melt front had a direct effect on the two-dimensional distribution of the core material as well as on the wall thickness of the core and skin materials. To trace the skin/core interface during the sequential injection of core polymer at a particular switch-over time after injection of skin polymer, Turng et al.[12–14] calculated the residence time of each material element based on the time and location at which the material element entered the cavity. Wang[15,16] employed the same approach to the consideration of simulating the injecting of two polymers in a sequential process without a delay time at the switch-over position. However, their model cannot be applied to the other type of coinjection process, simultaneous coinjection molding. Also, no detailed explanation of this residence time approach was given in their articles.[12–16] Chen et al.[17–19] also developed a simulation program. Theirs was based on a dual-filling-parameter particle-tracing scheme employed within each grid layer in the gapwise direction to trace the advance of the melt fronts for both the skin and core materials during the sequential coinjection process. Although all these studies were more focused on simulations of the flow front of both the skin and core components, an explanation of the interface treatment was not provided. It is our understanding that in their simulations the core component entering the cavity displaced the skin component in front of it by a steady-state plug-type flow. Therefore, a core thickness distribution had to be estimated beforehand.

Zoetelief et al.[20] studied multicomponent injection molding by using a conservation of identity (which may be a material, a color, a place, or a time of injection) method. They applied a semianalytical flow-front model for particle tracking in order to locate the position of each component and to predict the interface distribution during the process. The mathematical formulation of the particle-tracking problem resulted in hyperbolic (scalar) convection equations that were solved by the Streamline Upwind Petrov Galerkin (SUPG) finite-element method. Schlatter et al.[21] proposed a thermomechanical model describing the sequential flow of the two polymers into the mold cavity based on the Hele–Shaw approximation. A transport equation characterizing the displacement of the interface between the two melts was employed. The governing equations were solved using a modified finite-volume scheme based on discontinuous Galerkin formulation. This model was also employed with an unsteady multifluid flow during sequential sandwich injection molding.[22] Their model did not take into account the breakthrough phenomena and the interfacial instabilities. Also, in their calculation the polymer melts were assumed to follow power-law shear-thinning behavior. Actually, the simulation showed that the shear rates were very low near the wall and in the center region, so the use of the power-law model might be one of the reasons for the difference between the experimental results and their simulation. Nevertheless, numerical simulation was able to qualitatively predict the trend of interface evolution observed in the experiments. Palluch and Isayev[23] calculated a one-dimensional two-layer flow of viscoelastic polymer melts in sequential coinjection molding with the transient interface movement, and they predicted the stress-induced crystallization within the semicrystalline polymers. The effect of elasticity on the interface development was also taken into account in their model. However, their theoretical model has not been verified by comparing the simulation results with experimental data. Lee et al.[24] assumed a steady-state plug-type core melt flow during the cavity filling and calculated a one-dimensional interface distribution between the two phases in the simultaneous sandwich injection molding.

In the coinjection-molding process the effects of material properties and processing parameters on the structure and distribution of each component are interdependent and coupled with cavity geometry and a gating system. Because of the dynamic interaction of the two polymers in the manufacturing process and the difference in their properties, process control becomes more complicated, and thus process design becomes more challenging. The procedures used for the conventional single-phase injection-molding process design,[25–27] which have been well described, may not always be useful for coinjection molding. The numerical model and simulation that specifically targeted the multicomponent process need to be developed further. Surprisingly, the existing literature does

not provide a detailed description of the interface treatments during the multicomponent molding process.

Therefore, the attempt of the present study was to systematically describe a physical model and process simulation of coinjection molding based on the kinematics and dynamics of the interface evolution as well as the Hele–Shaw approximation. This study considered the simultaneous coinjection of both skin and core polymers in a flow-rate-controlled process with a certain amount of skin polymer injected first. However, this process also could be utilized for other multicomponent processes, such as sequential coinjection and pressure-controlled processes.

KINEMATICS AND DYNAMICS OF INTERFACE EVOLUTION

The specific problem in coinjection molding is tracking the evolution of the interface such that a predictive computation can be useful for reaching the optimum material configuration and encapsulated sandwich structure. Thus, the physicochemical transport equations that describe the interface characteristics should be well established from the fluid dynamic and from both interfacial kinematic and dynamic viewpoints because the location of the interface strongly depends on the individual polymer's rheological properties and their interaction, as well as on the processing conditions.

Because of the time-dependent transient interface evolution between the skin and core, the interface is considered an internal moving boundary whose condition is defined along the topological interface between two flow subdomains and whose position is not known in advance and thus must be computed as a part of the solution. Therefore, moving-boundary problems have additional degrees of freedom and additional equations, compared with fixed-boundary flow problems. The quantitative description of such problems depends on understanding the physical processes taking place on the interface and on the successful solution of the corresponding moving-boundary problems. The current knowledge in both these areas is far from complete.[28,29] Generally, two requirements that must be satisfied are the kinematic condition and the dynamic condition.

The kinematic condition

The time-dependent kinematic condition must relate the change of the moving interface position to the local velocity. Therefore, to determine the new transient interface locations, the nodes on the interface are supposed to deform in accordance with the instantaneous velocity field at the interface. In general, the moving interface can be considered as a three-dimensional

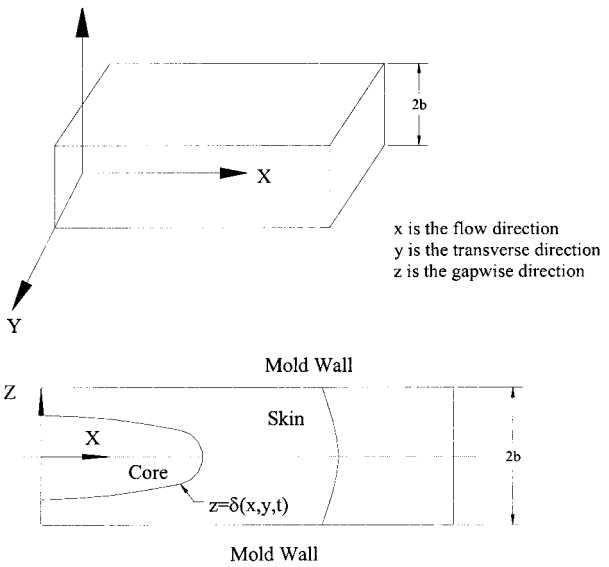

Figure 1 Coordinate system in coinjection molding cavity along with the schematic of the two-melt flow.

streaming surface along which particles move. Thus, from the kinematic point of view, the interface evolution can be represented by the following equation (Fig. 1):

$$z = \delta(x, y, t) \tag{1}$$

where z is the interface location between two flow subdomains.

Because material points move with the interface, the conservation of mass at the moving interface should be satisfied at any time. Then, in the absence of surface tension the rate of displacement of the moving interface is related to the fluid velocity, $\vec{V}_i(u, v, w)$ at the interface through the following equation:

$$w_i^\delta = \frac{D\delta}{Dt} = \frac{\partial \delta}{\partial t} + \vec{V}_i^\delta \cdot \nabla \delta \tag{2}$$

where w_i^δ is the velocity component in the thickness direction at the interface.

For a thin plate or strip cavity of the molding process where the Hele–Shaw approximation is applied, the two-dimensional planar flow is generally of main concern. Flow in the thickness direction is insignificant, meaning that w_i^δ. Therefore, for time-dependent problems, the above kinematic condition of the moving interface becomes

$$\frac{\partial \delta}{\partial t} + u_i^\delta \frac{\partial \delta}{\partial x} + v_i^\delta \frac{\partial \delta}{\partial y} = 0 \tag{3}$$

where u_i^δ; v_i^δ is the skin/core velocity at the interface; i is the skin or core polymer, respectively; and δ is the interface position between the skin and core melt.

Equation (3) states that a time-dependent moving boundary must follow trajectories in the normal direction and that no mass can cross the moving interface—in other words, the direction in which interface nodes are allowed to move never becomes tangent to the moving interface, which is evaluated as a function of the solution itself.

For a steady-state moving interface, the above kinematic equation reduces to

$$\vec{V}_i^{\delta} \cdot \vec{n} = 0 \tag{4}$$

where $\vec{n}$ is the unit normal vector to the interface.

Apparently, the position of the steady-state moving interface must be prescribed upstream of the moving interface.

The dynamic conditions

In the coinjection-molding process, a sharp interface is assumed to exist between the skin and the core materials, which means there is no macroscopic mixing at the interface. Therefore, the continuity of the velocity, $\vec{V}_i$, and the total stress tensor, $\tilde{\tilde{\sigma}}_i$, across the skin–core interface should be satisfied, that is:

$$\vec{V}_c^{\delta} = \vec{V}_s^{\delta} \tag{5}$$

$$\tilde{\tilde{\sigma}}_c^{\delta} = \tilde{\tilde{\sigma}}_s^{\delta} \tag{6}$$

where

$$\tilde{\tilde{\sigma}} = -p\tilde{\tilde{I}} + \tilde{\tilde{\tau}} \tag{7}$$

where the subscripts c and s denote the core and skin, respectively, p is the hydrostatic pressure, $\tilde{\tilde{\tau}}$ is the extra or viscous stress tensor, $\tilde{\tilde{I}}$ is the unit tensor, and $\tilde{\tilde{\sigma}}$ is the total stress tensor.

Fundamental studies of stratified two-phase polymer melt flow reported by White et al.[30–37] and Han et al.[38–41] provide some understanding of the effects of rheological properties on the interface shape in this process. From their theoretical analysis they concluded that viscosity played a predominant role over elasticity in determining the equilibrium interface shape between two fluids. Only for fluids of equal viscosities is the second difference of normal stresses contribute able to contribute to the interface distribution, as shown by White et al.,[32] who examined theoretically the two-phase isothermal flow of viscoelastic melts.

In this study an inelastic non-Newtonian fluid was assumed, along with the Hele–Shaw approximation. Thus, it can be assumed that the pressure and the shear stress are continuous at the interface. Then eq. (7) can be reduced to

$$\left(\eta \frac{\partial \vec{V}}{\partial z}\right)_c = \left(\eta \frac{\partial \vec{V}}{\partial z}\right)_s \tag{8}$$

COINJECTION MOLDING PROCESS SIMULATION

Governing transport equations

The flow mechanism depends on the corresponding properties of both the skin and core materials. Because of the dynamic interaction (mass, heat, and momentum) of these two polymers and the differences in the rheological and thermal properties during the coinjection-molding process, the rules used for the traditional single-phase injection-molding process design may not always be suitable for coinjection molding. The numerical simulation should be able to differentiate the materials at any instant and location in the cavity. Therefore, to track the interface shape, tracing individual components is required during the entire molding process.

In the present implementation for the coinjection-molding process, each polymer obeys the governing equations for generalized Hele–Shaw flow of inelastic, non-Newtonian fluids under nonisothermal conditions, with the following generally accepted assumptions about the governing transport equations, which are made for simplification:

- The polymeric liquids are incompressible, and the effects of gravitational and inertial forces are negligible because of the small Reynolds number.
- The lubrication approximation theory is applied, and the velocity and dynamic forces in the gapwise direction are neglected because the thickness is very thin.
- There is no slip at the wall.
- The pressure is assigned as zero at the skin melt front.
- The fountain flow effect at the melt front is not taken into account.
- Thermal convection in the gapwise direction is negligible.
- Heat evolution from crystallization of the semicrystalline polymers and from vulcanization of the rubber compound is neglected.
- A sharp interface is assumed to exist between the skin and core fluids. The fluids are not miscible at the interface.

The interface instabilities[42] between the polymer melts are not addressed here. The above assumptions lead to a Hele–Shaw type flow of the polymer melt, with the pressure independent of the gapwise position. The governing transport equations are

$$\nabla p = \frac{\partial}{\partial z}\left(\eta_i \frac{\partial \vec{V}_i}{\partial z}\right) \tag{9}$$

$$\frac{\partial u_i}{\partial x} + \frac{\partial \nu_i}{\partial y} = 0 \tag{10}$$

$$\rho_i C_{p,i}\left(\frac{\partial T}{\partial t} + u_i \frac{\partial T}{\partial x} + \nu_i \frac{\partial T}{\partial y}\right) = k_i \frac{\partial^2 T}{\partial z^2} + \eta_i \dot{\gamma}_i^2 \tag{11}$$

with

$$\nabla p = \begin{bmatrix} \dfrac{\partial p}{\partial x} \\ \dfrac{\partial p}{\partial y} \end{bmatrix} \quad \text{and} \quad \vec{V} = \begin{bmatrix} u \\ \nu \end{bmatrix}$$

where x, y, and z are the flow, width, and thickness directions, respectively; p, T, u, and v represent the pressure, temperature, and melt velocities in the x and y directions, respectively; b is the half-gap thickness of the mold cavity, which may be a function of x and y; and $\dot{\gamma}_i$, η_i, ρ_i, $C_{p,i}$, and k_i represent the shear rate, viscosity, density, specific heat, and thermal conductivity of the skin or core material respectively, depending on the region where these equations are applied.

For an inelastic non-Newtonian fluid, the modified four-parameter Cross model[43] is employed:

$$\eta(T, \dot{\gamma}) = \frac{\eta_0(T)}{1 + (\eta_0(T)\dot{\gamma}/\tau^*)^{1-n}} \tag{12}$$

where η_0 is the zero shear viscosity, τ^* is the shear-stress level at which η is in transition between the Newtonian limit, η_0, and the power-law region. The zero shear rate viscosity is defined as $\eta_0(T) = A \exp(T_b/T)$, where A is a preexponent for the viscosity–temperature function and T_b is a measure of the temperature sensitivity of the viscosity.

The boundary and initial conditions are

$$u|_{z=\pm b} = \nu|_{z=\pm b} = 0 \tag{13}$$

$$\left.\frac{\partial u}{\partial z}\right|_{z=0} = \left.\frac{\partial \nu}{\partial z}\right|_{z=0} = 0 \tag{14}$$

$$T|_{z=\pm b} = T_w \tag{15}$$

$$\left.\frac{\partial T}{\partial z}\right|_{z=0} = 0 \tag{16}$$

$$T = T_m \quad \text{at} \quad t = 0 \tag{17}$$

$$\frac{\partial p}{\partial n} = 0 \quad \text{no penetration at all solid boundaries} \tag{18}$$

$$p = p_{ent} \quad \text{or} \quad Q = Q_{ent} \quad \text{at the gate} \tag{19}$$

Although the solution of kinematic eq. (3) leads to the exact location of the moving interface, its determination is not obvious. Thus, further effort is necessary to incorporate the kinematic and dynamic equations with the conservation equations of fluid (mass and momentum equations). For the incompressible flow during the filling stage, integrating the mass continuity equation over the core layer thickness leads to

$$\int_0^\delta \frac{\partial u_c}{\partial x}\, dz + \int_0^\delta \frac{\partial \nu_c}{\partial y}\, dz = 0 \tag{20}$$

The local flow rates per unit width in the x and y directions are

$$q_x^c = \int_0^\delta u_c dz = \delta \cdot \bar{u}_c \tag{21}$$

$$q_y^c = \int_0^\delta \nu_c dz = \delta \cdot \bar{\nu}_c \tag{22}$$

where $\bar{u}_c$ and $\bar{\nu}_c$ are the average velocities of core material in the x and y directions, respectively.

The derivatives of eqs. (21) and (22) with respect to x and y are

$$\frac{\partial q_x}{\partial x} = \int_0^\delta \frac{\partial u_c(x, y, z)}{\partial x}\, dz + u_c^\delta \cdot \frac{\partial \delta}{\partial x} \tag{23}$$

$$\frac{\partial q_y}{\partial y} = \int_0^\delta \frac{\partial \nu_c(x, y, z)}{\partial y}\, dz + \nu_c^\delta \cdot \frac{\partial \delta}{\partial y} \tag{24}$$

Combining eqs. (20), (23), and (24) leads to

$$\frac{\partial q_x^c}{\partial x} + \frac{\partial q_y^c}{\partial y} = \vec{V}_c^\delta \cdot \nabla \delta = u_c^\delta \cdot \frac{\partial \delta}{\partial x} + \nu_c^\delta \cdot \frac{\partial \delta}{\partial y} \tag{25}$$

where u_c^δ and v_c^δ are the core melt velocity components at the interface, δ.

Following the same procedure for the skin material, it is possible to obtain

$$\frac{\partial q_x^s}{\partial x} + \frac{\partial q_y^s}{\partial y} = -\vec{V}_s^\delta \cdot \nabla \delta = -\left[u_s^\delta \cdot \frac{\partial \delta}{\partial x} + \nu_s^\delta \cdot \frac{\partial \delta}{\partial y}\right] \tag{26}$$

where u_s^δ and v_s^δ are the skin melt velocity components at the interface, δ.

By adding eq. (25) to eq. (26), the mass balance equation as a function of the whole gapwise-averaged velocity, $\bar{\vec{V}}(\bar{u}, \bar{\nu})$, can be obtained:

$$\nabla \cdot (b\overrightarrow{\overrightarrow{V}}) = 0, \tag{27}$$

where

$$\overrightarrow{\overrightarrow{V}} = \frac{\int_0^\delta \overrightarrow{V}_c dz + \int_\delta^b \overrightarrow{V}_s dz}{b}. \tag{28}$$

Using the concept of average velocity over the layer thickness of each material (skin/core) as given by eqs. (21) and (22), eqs. (25) and (26) can be written in the form:
For the core polymer—

$$\nabla \cdot (\delta \overrightarrow{\overrightarrow{V}}_c) = \overrightarrow{V}_c^{\,\delta} \cdot \nabla \delta \tag{29}$$

For the skin polymer—

$$\nabla \cdot [(b - \delta) \overrightarrow{\overrightarrow{V}}_s] = \overrightarrow{V}_s^{\,\delta} \cdot \nabla (b - \delta) \tag{30}$$

Considering eq. (3), eqs. (29) and (30) can also be written as, respectively:

$$\nabla \cdot (\delta \overrightarrow{\overrightarrow{V}}_c) = -\frac{\partial \delta}{\partial t} \tag{31}$$

$$\nabla \cdot [(b - \delta) \overrightarrow{\overrightarrow{V}}_s] = \frac{\partial \delta}{\partial t} \tag{32}$$

Thus, eqs. (29) and (30) or eqs. (31) and (32) let each material layer (skin/core) satisfy the mass continuity, with eq. (27) satisfying the total mass continuity. It should be mentioned that eq. (32) was derived based on the assumption that the gapwise velocity, w_i^δ, = 0. However, as indicated in the Appendix, this equation also can be obtained without making this assumption.

After the integration of eq. (9) over the thickness of the skin and core polymers, respectively, with the use of the symmetry boundary condition at the center line, the following relationship between the skin and core polymers is obtained

$$\nabla p \cdot z = \eta_i \left. \frac{\partial \vec{V}_i}{\partial z} \right|_z \tag{33}$$

for the core polymer and for the skin polymer.

The integration of eq. (33) over each layer thickness produces the relationship between the velocities at the interface of the skin/core polymer and at the central line. The use of the boundary condition of no slip at the wall leads to the following equations:

$$\nabla p \int_0^z \frac{z}{\eta_c} dz = \vec{V}_c|_z - \vec{V}_c|_{z=0} \tag{34}$$

for the core fluid, $0 \le z \le \delta$.
and

$$\nabla p \int_z^b \frac{z}{\eta_s} dz = -\vec{V}_s|_z \tag{35}$$

for the skin fluid, $\delta \le z \le b$.

Given the continuity of the velocity at the interface, $z = \delta$, that is, eq. (5), it is possible to obtain

$$\vec{V}_c|_{z=0} = \nabla p \left[\int_0^\delta \frac{z}{\eta_c} dz + \int_\delta^b \frac{z}{\eta_s} dz \right] \tag{36}$$

Finally, a further integration of eq. (36) over the skin and core polymer thicknesses, respectively, with the use of the continuity of the shear stress and of the velocity at the interface between the skin and core materials [eqs. (5) and (8)] leads to the following expressions for the average velocity, $\bar{V}_c$ and $\bar{V}_s$.
for the core polymer:

$$\delta \overrightarrow{\overrightarrow{V}}_c = -\nabla p \int_0^\delta \left[\int_z^\delta \frac{z}{\eta_c} dz + \int_\delta^b \frac{z}{\eta_s} dz \right] dz' \tag{37}$$

or

$$\delta \overrightarrow{\overrightarrow{V}}_c = -\nabla p \cdot S_c \tag{38}$$

with

$$S_c = \int_0^\delta \frac{z^2}{\eta_c} dz + \delta \int_\delta^b \frac{z}{\eta_s} dz \tag{39}$$

for the skin polymer:

$$(b - \delta) \overrightarrow{\overrightarrow{V}}_s = -\nabla p \int_\delta^b \int_z^b \frac{z}{\eta_s} dz dz' \tag{40}$$

or

$$(b - \delta) \overrightarrow{\overrightarrow{V}}_s = -\nabla p \cdot S_s \tag{41}$$

with

$$S_s = \int_{\delta}^{b} \frac{z(z-\delta)}{\eta_s}\, dz. \tag{42}$$

Combining eqs. (29) and (30) or eqs. (31) and (32) with eqs. (38) and (41) leads to
for the core melt

$$\frac{\partial \delta}{\partial t} + \frac{\partial}{\partial x}\left(-S_c \frac{\partial p}{\partial x}\right) + \frac{\partial}{\partial y}\left(-S_c \frac{\partial p}{\partial y}\right) = 0 \tag{43}$$

or

$$\vec{V}_c^{\delta} \cdot \nabla \delta + \frac{\partial}{\partial x}\left(S_c \frac{\partial p}{\partial x}\right) + \frac{\partial}{\partial y}\left(S_c \frac{\partial p}{\partial y}\right) = 0 \tag{44}$$

for the skin melt

$$\frac{\partial (b-\delta)}{\partial t} + \frac{\partial}{\partial x}\left(-S_x \frac{\partial p}{\partial x}\right) + \frac{\partial}{\partial y}\left(-S_s \frac{\partial p}{\partial y}\right) = 0 \tag{45}$$

or

$$\vec{V}_s^{\delta} \cdot \nabla (b-\delta) + \frac{\partial}{\partial x}\left(S_s \frac{\partial p}{\partial x}\right) + \frac{\partial}{\partial y}\left(S_s \frac{\partial p}{\partial y}\right) = 0 \tag{46}$$

These are the transient interface evolution equations for the interface tracking. It should be mentioned that an interface transport equation similar to eq. (44) also is used by Schlatter et al.[21,22] and Palluch and Isayev.[23] Adding eq. (43) to eq. (45) or adding eq. (44) to eq. (46) gives the following well-known Hele–Shaw type of governing equation for both materials in the whole cavity domain, which can be used to solve the pressure gradient distribution and velocity field:

$$\frac{\partial}{\partial x}\left(S \frac{\partial p}{\partial x}\right) + \frac{\partial}{\partial y}\left(S \frac{\partial p}{\partial y}\right) = 0 \tag{47}$$

where

$$S = \int_{0}^{\delta} \frac{z^2}{\eta_c}\, dz + \int_{\delta}^{b} \frac{z^2}{\eta_s}\, dz \tag{48}$$

where δ is the half thickness of the core melt in the gapwise direction and η_c and η_s are the viscosity for the core and skin melts, respectively. At $\delta = 0$, eq. (47) reduces to the governing equation for the single-phase injection molding.

Numerical formulation and simulation

The governing equations coupled with the nonlinear viscosity function need to be solved numerically in order to determine the pressure, flow rate, velocity, shear rate, viscosity, and shear stress profiles, as well to ascertain the interface distribution and the melt-front advancement. However, these equations are highly nonlinear in nature. Thus, the approach based on a hybrid control-volume finite-element and finite-difference method (CV/FEM/FDM)[26,44–47] is employed to solve these problems by using successive underrelaxation iteration.

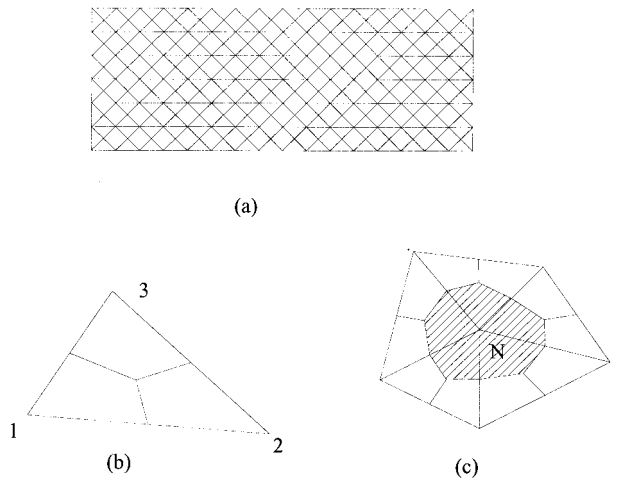

Figure 2 (a) Three-node triangular elements in planar direction. (b) Three-node triangular element and subcontrol volumes associated with the element. (c) Control volume associated with node N.

For a two-dimensional flow, the whole domain is made into a series of discrete three-node triangular elements in the x–y plane [Fig. 2(a,b)]. Each finite element has a constant thickness. Only one control volume is associated with each node. By connecting the centroid of each triangular element to its midpoint, the subcontrol volume for each node of this element is specified as the region enclosed by a contour in the counterclockwise direction around each vertex node of the triangular element [Fig. 2(c)].

The pressure and interface distribution on each element can be expressed by the nodal pressures and nodal interface position by the corresponding linear interpolation functions:

$$p(x, t) = \sum_{j=1}^{2 \text{ or } 3} L_j^l(x) p_j^l(t) \tag{49}$$

$$\delta(x, t) = \sum_{j=1}^{2 \text{ or } 3} L_j^l(x) \delta_j^l(t), \tag{50}$$

where $L_j^l(x)$ is the linear area–coordinate interpolation function for node j on element l[26,44–47] and $\delta_j^l(t)$ denotes the nodal pressures and the nodal interface positions. Moreover, it is reasonable to assume that S and

S_c are constant over each element, being evaluated at its centroid. After applying the Galerkin weighted-residual procedure[48,49] or mass conservation using a control-volume approach,[50] and introducing linear interpolation functions as well as a finite-difference representation for the time derivative, the following governing equation for pressure in the whole cavity domain is obtained:

$$\sum_{1}^{ku} \sum_{j=1}^{2 \text{ or } 3} S^l \tilde{\tilde{B}}^l_{i,j} p^l_{N'} = Q_N \tag{51}$$

where Q_N is the total volumetric flow rate for each node at any instant for the whole cavity domain, ku is the total number of elements containing node N, and i is such that $N = NELNOD(l,i)$ and $N' = NELNOD(l,j)$, with $j = 1,2$ for the strip elements. Also,

$Q_N = Q_{\text{ent}}$ for the entrance nodes where $p = p_g$ or $Q_{\text{ent}} = Q_g$ is specified at the gate;
$Q_N = 0$ for the internal fully filled nodes;
$Q_N = Q_{\text{out}}$ for the melt-front nodes where $p = 0$ is assumed.

Similarly, the interface evolution equation leads to the following numerical formulation:

$$\sum_{1}^{ku} \sum_{j=1}^{2 \text{ or } 3} \frac{d\delta_j}{dt} \tilde{\tilde{D}}_{i,j} A^l + \sum_{1}^{ku} \sum_{j=1}^{2 \text{ or } 3} S^l_c \tilde{\tilde{B}}^l_{i,j} p_{N'} = Q^c_N \tag{52}$$

where $N = NELNOD(i,j)$ and $N' = NELNOD(l,j)$ is the volumetric flow rate of the core component, which is different for the control volume associated with the different nodes. Similarly, it can be found that

$Q^c_N = Q^c_{ent}$ for the entrance nodes where $p = p_g$ or $Q^c_{ent} = Q^c_g$ is specified at the gate;
$Q^c_N = 0$ for the internal fully filled nodes;
$Q^c_N = Q^c_{out}$ for the melt-front nodes where $p \neq 0$.

In addition, A^1 is the area of each element associated with node N; $\tilde{\tilde{D}}_{i,j}$ and $\tilde{\tilde{B}}_{i,j}$ are the element matrices; and $\tilde{\tilde{B}}_{i,j}$ is the influence coefficient of the nodal pressure to the net flow rate in element l; and $\tilde{\tilde{D}}_{i,j}$ is the influence coefficient of the nodal interface location on the net flow rate in element l.

It should be noted that both eqs. (51) and (52) are based on the control-volume scheme, which must allow the strict conservation of the mass in all subdomains as well as in the main flow domain. Moreover, as both eqs. (51) and (52) are highly nonlinear mainly because of the dependency of S and S_c on the pressure field and interface profile, an iterative numerical procedure is required. Successive underrelaxation can be employed. In turn, this requires that S and S_c be updated after every few iterations of the nodal pressures and then of the nodal interface positions. As soon as the global convergence of both the pressure field and interface distribution is obtained, associated flow quantities such as velocity, shear rate, and viscosity can then be updated as well.

The volume of fluid (VOF) model,[51] with separate filling factor that varies between 0 and 1 for each component, is used to track the advance of the core (core/skin interface in planar direction) and the skin melt fronts. In the VOF model the fluid volume is represented by a characteristic filling parameter, F, by which the movement of the melt front is advected by the velocity field. This parameter, F, is governed by

$$\frac{\partial F_i}{\partial t} + \bar{V} \cdot \nabla F_i = 0 \tag{53}$$

The advection of the fluid volume is based on the mass conservation around each control volume. This conservation requires that the change in the filling factor of each melt-front node at each time step is proportional to the net flow rate of fluid into the control volume; thus,

$$F^{n+1}_i = F^n_i + \frac{\Sigma_j \, q_{i,j} \Delta t}{V_i} \tag{54}$$

where V_i is the total volume of the control volume associated with node i and $q_{i,j}$ is the flow rate of fluid entering each subcontrol volume of node i.

Once the filling factors of both the skin and core melts are updated using this equation, a new filled domain and subdomain can be defined with the advancement of both melt fronts for the next time step.

CONCLUSIONS

A physical modeling and numerical simulation procedures of coinjection molding has been developed based on the Hele–Shaw approximation, combined with the kinematics and dynamics of the time-dependent moving interface. The transient gapwise interface development during coinjection molding can be described by the interface evolution equation formulated in this study. Both core and skin melt-front advancement are tracked by employing the volume of fluid (VOF) model. The hybrid control-volume finite-element method and finite-difference method (CV/FEM/FDM) is employed to solve the formulated governing equations for pressure and interface distribution coupled with nonlinear shear viscosity function, which is described by the modified temperature-dependent Cross model. Based on this developed numerical model, the simulation results and experimen-

tal data will be compared in the upcoming second part of this series in order to verify the validity of the model. In addition, the effects of material combinations and processing parameters on the phase distribution and interface shape will be evaluated.

APPENDIX

Interface evolution for the case of nonzero gapwise velocity

The moving interface is introduced as follows:

$$z = \delta(x, y, t) \tag{A-1}$$

Based on the kinematic boundary condition of the mass conservation at the moving interface, the local change of the interface position, δ, is given as

$$\frac{\partial \delta}{\partial t} = w_i^\delta - u_i^\delta \frac{\partial \delta}{\partial x} - \nu_i^\delta \frac{\partial \delta}{\partial y} = w_i^\delta - \vec{V}_i^\delta \cdot \nabla \delta \tag{A-2}$$

Mass continuity for skin/core subdomains is:

$$\frac{\partial u_i}{\partial x} + \frac{\partial \nu_i}{\partial y} + \frac{\partial w_i}{\partial z} = 0 \tag{A-3}$$

The integration of eq. (A.III) over the thickness of the core region results in

$$\int_0^\delta \frac{\partial u_c}{\partial x}\, dz + \int_0^\delta \frac{\partial \nu_c}{\partial y}\, dz + w_c^\delta - w_c^{z=0} = 0 \tag{A-4}$$

At the center of cavity, $w = 0$; therefore, eq. (A.IV) reduces to

$$\int_0^\delta \frac{\partial u_c}{\partial x}\, dz + \int_0^\delta \frac{\partial \nu_c}{\partial y}\, dz = -w_c^\delta \tag{A-5}$$

From eqs. (23) and (24) in the main text, the local flow rate change in core region can be written as

$$\frac{\partial q_x^c}{\partial x} + \frac{\partial q_y^c}{\partial y} = \nabla \cdot (\delta \overrightarrow{\overrightarrow{V}}_c) = \int_0^\delta \frac{\partial u_c}{\partial x}\, dz + \int_0^\delta \frac{\partial \nu_c}{\partial y} + \overrightarrow{V}_c^\delta \cdot \nabla \delta \tag{A-6}$$

Combining eqs. (A.V) and (A.VI) leads to

$$\nabla \cdot (\delta \overrightarrow{\overrightarrow{V}}_c) = -w_c^\delta + \overrightarrow{V}_c^\delta \cdot \nabla \delta \tag{A-7}$$

Using eq. (A.II), the above equation can be written as

$$\nabla \cdot (\delta \overrightarrow{\overrightarrow{V}}_c) = -\frac{\partial \delta}{\partial t} \tag{A-8}$$

which is the same equation as eq. (31).

By applying a similar procedure to the skin region, it is possible to obtain

$$\nabla \cdot [(b - \delta) \overrightarrow{\overrightarrow{V}}_s] = \frac{\partial \delta}{\partial t} \tag{A-9}$$

This equation is the same as eq. (32).

References

1. Garner, P. J.; Oxley, D. F. Brit. Pat. 1,156,217 (1969).
2. Garner, P. J. U.S. Pat. 3,690,797 (1972).
3. Garner, P. J. U.S. Pat. 3,599,290 (1971).
4. Hanning, R. Ger. Offen. 2,241,002 [GB 1,399,279] (1973).
5. Langecker, E. Ger. Offen. 2,247,995 [GB 1,428,789] (1974).
6. Fillman, W.; Eckardt, H. Ger. Offen. 2,342,957 [GB 1,441,347] (1975).
7. Selden, R. J Inj Mold Technol 1997, 1, 189.
8. Somnuk, P.; Smith, G. F. SPE ANTEC 1995, 41, 760.
9. Lanvers, A.; Michaeli, W. SPE ANTEC 1992, 38, 1796.
10. Lanvers, A.; Galuschka, S.; Tietz, W. Eng Plast 1994, 7, 223.
11. Michaeli, W.; Galuschka, S. SPE ANTEC 1994, 40, 565.
12. Turng, L. S.; Wang, V. W. SPE ANTEC 1991, 37, 297.
13. Turng, L. S.; Wang, V. W.; Wang, K. K. HTD, 175/MD, 25, Heat and Mass Trans Solid Proc ASME 1991, 113.
14. Turng, L. S.; Wang, V. W.; Wang, K. K. J Eng Mat Tech 1993, 115, 48.
15. Wang, J. T. Am Soc Mech Eng 2000, 90, 257.
16. Wang, J. T. SPE ANTEC 2001, 47, 746.
17. Chen, S. C.; Hsu, K. F. Num Heat Trans, Part A 1995, 28, 503.
18. Chen, S. C.; Chen, N. T.; Hsu, K. S.; Hsu, K. F. AIChE J 1996, 42, 1706.
19. Chen, S. C.; Hsu, K. F.; Hsu, K. S.; Jeng, M. C. SPE ANTEC 1993, 39, 82.
20. Zoetelief, W. F.; Peters, G. W. M.; Meijer, H. E. H. Intern Polym Proces 1997, XII, 216.
21. Schlatter, G.; Davidoff, A.; Agassant, J. F.; Vincent, M. SPE ANTEC 1995, 43, 456.
22. Schlatter, G.; Agassant, J. F.; Davidoff, A.; Vincent, M. Polym Eng Sci 1999, 39, 78.
23. Palluch, K. P.; Isayev, A. I. SPE ANTEC 2000, 46, 528.
24. Lee, D. J.; Isayev, A. I.; White, J. L. SPE ANTEC 1998, 44, 346.
25. Isayev, A. I., Ed. Injection and Compression Molding Fundamentals; Marcel Dekker: New York, 1987.
26. Isayev, A. I., Ed. Modeling of Polymer Processing; Oxford University Press: New York, 1991.
27. Kennedy, P. Flow Analysis of Injection Molds; Hanser Munich: New York, 1995.
28. Yeung, R. W. Ann Rev Fluid Mech 1982, 14, 395.
29. Floryan, J. M.; Rasmussen, H. Appl Mech Rev 1989, 42, 323.
30. Lee, B. L.; White, J. L. Trans Soc Rheol 1974, 18, 467.
31. Minagawa, N.; White, J. L. Polym Eng Sci 1975, 15, 825.
32. White, J. L.; Ufford, R. C.; Dhard, K. R.; Price, R. L. J Appl Polym 1972, 16, 1313.
33. White, J. L.; Lee, B. L. Trans Soc Rheol 1975, 19, 457.
34. White, J. L.; Lee, B. L. Polym Eng Sci 1975, 15, 481.
35. Young, S. S.; White, J. L.; Clark, E. S.; Oyanagi, Y. Polym Eng Sci 1980, 20, 798.
36. White, J. L.; Dee, H. B. Polym Eng Sci 1974, 14, 212.

37. Young, S. S.; White, J. L.; Clark, E. S.; Oyanagi, Y. SPE ANTEC 1980, 26, 163.
38. Yu, T. C.; Han, C. D. J Appl Polym Sci 1973, 17, 1203.
39. Han, C. D. J Appl Polym Sci 1973, 17, 1289.
40. Han, C. D. J Appl Polym Sci 1975, 19, 1875.
41. Khan, A. A.; Han, C. D. Trans Soc Rheol 1976, 20, 595.
42. Palluch, K. P.; Isayev, A. I. In Proceedings of the XIIIth International Congress on Rheology; 2000; p 213.
43. Cross, M. M. Rheol Acta 1979, 18, 609.
44. Hieber, C. A.; Shen, S. F. Israel J Technol 1978, 16, 248.
45. Hieber, C. A.; Shen, S. F. J Non-Newtonian Fluid Mech 1980, 7, 1.
46. Wang, V. W.; Hieber, C. A.; Wang, K. K. J Polym Eng 1986, 7, 21.
47. Wang, V. W.; Hieber, C. A.; Wang, K. K. SPE ANTEC 1986, 32, 97.
48. Huebner, K. H.; Thornton, E. A.; Byrom, T. G. Wiley: New York, 1995.
49. Zienkiewicz, O. C. The Finite Element Method, 3rd ed.; McGraw-Hill: New York, 1977.
50. Winslow, A. M. J Comp Phys 1967, 2, 149.
51. Hirt, C. W.; Nichols, B. D. J Comp Phys 1981, 39, 201.